XII International Conference on Computational Plasticity. Fundamentals and Applications
COMPLAS XII
E. Oñate, D.R.J. Owen, D. Peric and B. Suárez (Eds)

MODELING OF HIGH SPEED FRICTION STIR SPOT WELDING USING A LAGRANGIAN FINITE ELEMENT APPROACH

M.P. MILES[*], U. KARKI[*] C. WOODWARD[*], AND Y. HOVANSKI[†]

[*] Manufacturing Engineering Technology
Brigham Young University, Provo, UT 84602, USA
email: mmiles@byu.edu

[†] Pacific Northwest National Lab
Richland, WA 99352

Key words: Friction Stir Spot Welding, Lagrangian Finite Element Method, Advanced High Strength Steel

Abstract. Friction stir spot welding (FSSW) has been shown to be capable of joining steels of very high strength, while also being very flexible in terms of controlling the heat of welding and the resulting microstructure of the joint. This makes FSSW a potential alternative to resistance spot welding (RSW) if tool life is sufficiently high, and if machine spindle loads are sufficiently low so that the process can be implemented on an industrial robot. Robots for spot welding can typically sustain vertical loads of about 8kN, but FSSW at tool speeds of less than 3000 rpm cause loads that are too high, in the range of 11-14 kN. Therefore, in the current work tool speeds of 3000 rpm and higher were employed, in order to generate heat more quickly and to reduce welding loads to acceptable levels. The FSSW process was modeled using a finite element approach with the Forge® software package. An updated Lagrangian scheme with explicit time integration was employed to model the flow of the sheet material, subjected to boundary conditions of a rotating tool and a fixed backing plate [3]. The modeling approach can be described as two-dimensional, axisymmetric, but with an aspect of three dimensions in terms of thermal boundary conditions. Material flow was calculated from a velocity field which was two dimensional, but heat generated by friction was computed using a virtual rotational velocity component from the tool surface. An isotropic, viscoplastic Norton-Hoff law was used to model the evolution of material flow stress as a function of strain, strain rate, and temperature. The model predicted welding temperatures and the movement of the joint interface with reasonable accuracy for the welding of a dual phase 980 steel.

1 INTRODUCTION

Friction stir welding (FSW) and friction stir spot welding (FSSW) have been studied extensively for joining of aluminum alloys, whereas the volume of work done in steel has been much less. One of the reasons for this is the difficulty of developing a tool which can survive the high stresses and temperatures of welding steel [1]. Despite this challenge, there has been some progress on FSW and FSSW of steels, primarily during the past 6-7 years. For

example, FSW work on dual phase (DP) 590 sheets showed that weld hardness can be adjusted up or down, by changing the feeds and speeds of the welding tool in order to target a given welding temperature [2-5]. In contrast to this, a conventional fusion welding process, like laser welding, produces a very hard weld in DP 590 sheets, with much less formability than friction stir welded sheets when the weld is stretched in a forming operation, as needed for tailor welded blanks [2]. The heat of welding during FSW or FSSW in steel is usually in the range of 900-1200˚C, which is significantly below the melting point of steel of about 1500˚C. A lower heat of welding can be an advantage in limiting the extent of the heat affected zone (HAZ), which is exploited when stresses are applied across the joint, causing deformation to localize where softening has occurred [2, 3, 6]. However, because the heat of welding in FSW and FSSW is adjustable, the extent of the HAZ depends on the welding parameters and can vary significantly.

While there are similarities between FSW and FSSW of steel, FSSW is quite different from a process viewpoint. FSSW is a stationary plunge of the tool, creating a spot weld in lap configuration, while FSW is used to make a seam weld in either butt or lap configurations. Like FSW, FSSW has been shown to be capable of joining steels of very high strength, while also being very flexible in terms of controlling the heat of welding and the resulting microstructure of the joint [7-11]. This makes FSSW a potential alternative to resistance spot welding (RSW) if tool life is sufficiently high, and if machine spindle loads are sufficiently low. Industrial robots for spot welding can typically sustain vertical loads of about 8kN, so FSSW at tool speeds of less than 3000 rpm cause loads that are too high, in the range of 11-14 kN. Therefore, in the current work tool speeds of 3000 rpm and higher were employed, in order to produce heat more quickly and to reduce welding loads to acceptable levels. There are several tool materials which have been tried for FSSW of AHSS, including silicon nitride (Si_3N_4), polycrystalline cubic boron nitride (PCBN), tungsten rhenium (W-Re), tungsten carbide (WC), and other tungsten-based alloys [2-8, 12-14]. Some indication of wear resistance has been given in prior work, showing that PCBN tools had less wear than W-Re or Si_3N_4 tools for a limited number of welds, in the range of several hundred spots [7-9]. However, Si_3N_4 tools can be produced relatively inexpensively, so Si_3N_4 is the tool material that was evaluated in the current study.

Relatively little modeling effort has been focused on FSSW thus far. Unlike FSW, which can be approximated as a steady-state process, FSSW is a non steady state process and must be modeled by an approach that takes into account the evolving nature of material flow and heat generation. Therefore, an updated Lagrangian or an arbitrary Lagrangian Eulerian (ALE) formulation is more appropriate for modeling of FSSW, using a material law that provides flow stress as a function of strain, strain rate, and temperature. As such, there has been some prior work where FSSW has been modeled using a Lagrangian finite element approach [15, 16]. A Lagrangian approach will be described in this paper, where the velocity field in the sheet will modeled as two-dimensional, axisymmetric. The temperature computation will also be two-dimensional, but the frictional heat at the tool/sheet interface will be computed based on the rotational velocity of the tool.

2 EXPERIMENTAL METHODS

Welding experiments employed tool speeds of 3000 – 6000 rpm on a Fadal machining center, where the lap shear tension configuration was used to evaluate joint strength. Lap shear specimens were made using coupons of 1.2 mm bare dual phase (DP) 980 steel, with dimensions of 25 mm by 100 mm, and an overlap of 25 mm. The DP 980 steel composition, in weight percent, was 0.15% C, 1.44% Mn, 0.011% P, 0.007% S, 0.32% Si, and 0.02% Cr, where the balance was Fe. The spot weld was positioned in the center of the overlap in each case. Si_3N_4 tools with a shoulder diameter of 10 mm and a smooth pin, with three small flats, were used for all spot welding experiments. The flats tended to wear off quickly, leaving a completely smooth pin after approximately 10 welds.

3 DESCRIPTION OF FRICTION STIR SPOT WELDING MODEL

Modeling was done using a finite element approach with the Forge® [17] software package. An updated Lagrangian scheme was employed to model the flow of the sheet material, subjected to boundary conditions of a rotating tool and a fixed backing plate. The modeling approach can be described as two-dimensional, axisymmetric, but with an aspect of three dimensions in terms of thermal boundary conditions. Material flow was calculated from a velocity field that was two dimensional, but heat generated by friction was computed using the rotational velocity of the tool surface. An isotropic, viscoplastic Norton-Hoff law was used to model the evolution of material flow stress as a function of strain, strain rate, and temperature. The expression for the deviatoric stress tensor is shown below:

$$\boldsymbol{s} = 2K\left(\sqrt{3}\dot{\bar{\varepsilon}}\right)^{m-1}\dot{\boldsymbol{\varepsilon}} \tag{1}$$

where $\dot{\varepsilon}$ is the strain rate tensor, $\dot{\bar{\varepsilon}}$ is the effective strain rate, and K is the material consistency, and m is the strain rate sensitivity of the material. The material consistency K is a function of temperature T and equivalent strain $\bar{\varepsilon}$, where n is the strain hardening exponent and β is a thermal softening parameter, as seen in equation (2):

$$K = K_o(\varepsilon_o + \bar{\varepsilon})^n e^{\frac{\beta}{T}} \tag{2}$$

This viscoplastic law is capable of modeling material flow stresses in the region of the weld, while also providing the contact stresses used to calculate the friction shear stress at the tool/sheet interface. Friction conditions at the sliding interface between the sheet and the tool were modeled by the viscoplastic Norton law [18], where the friction shear stress is a function of sliding velocity:

$$\tau_f = -\alpha_f K \|\Delta \boldsymbol{v_s}\|^{p-1}\Delta \boldsymbol{v_s} \tag{3}$$

where α_f is the friction coefficient, K is the same material consistency shown in equation (2), $\Delta \boldsymbol{v_s}$ is the relative sliding velocity, and p is the rate sensitivity of the relative sliding velocity.

Calculation of material flow was based on a finite element discretization using an enhanced (P1+/P1) 3-noded triangular element [17], where equilibrium equations were solved at each increment using the Newton-Raphson method. The unilateral contact condition was applied to

the sheet surfaces by means of a nodal penalty formulation, where the FSSW tool and backing plate were considered rigid. An explicit time integration scheme was used to update the sheet geometry at each increment of calculation:

$$X_{t+\Delta t} = X_t + V_{mesh}\Delta t \tag{4}$$

where **X** is the mesh material coordinate, $\mathbf{V}_{mesh}$ is the velocity of the mesh at time t, and Δt is a time increment chosen sufficiently small. While the tool and backing plate were considered to be mechanically rigid, the evolution of temperature in the tool was modeled in order to provide accurate boundary conditions at the tool/sheet interface. The temperature in both the FSSW tool and the sheet were calculated at the end of each material flow increment. The calculated velocity field allowed for computing strain rates and stresses in the sheet, which were then used to determine the heat dissipated by friction and plastic deformation. The heat dissipation rate by plastic deformation is given by:

$$\dot{q}_p = f\bar{\sigma}\dot{\bar{\varepsilon}} \tag{5}$$

where $\bar{\sigma}$ is the equivalent stress and the factor f takes into account the fraction of deformation energy converted into heat, taken as 0.9 in this paper. For a Norton-Hoff viscoplastic material, the heat generation rate from material deformation is therefore determined as follows:
Heat from friction at the tool/sheet interface is given by:

$$\dot{q}_f = \boldsymbol{\tau} \cdot \Delta \boldsymbol{v_s} \tag{6}$$

where $\boldsymbol{\tau}$ is the friction shear stress from equation (3) and $\Delta \boldsymbol{v_s}$ is the relative sliding velocity at the sheet/tool interface. In the case of this axisymmetric model, the virtual velocity from the rotation of the tool is applied to equation (6) along the tool/sheet interface. Frictional heat is shared between the tool and the sheet as a function of the effusivities of each, where the material with higher effusivity receives a greater portion of the frictional heat. Effusivity is defined as $\sqrt{\rho c k}$, where ρ is density, c is heat capacity, and k is conductivity.

The boundary conditions for the backing plate were included in the model, based on thermocouple measurements that were done in prior work [18]. The thermal conductivity, heat capacity, and density of both the Si_3N_4 tool and the AHSS sheet were modeled as a function of temperature, over the range of temperatures from 25°C to 1400°C.

4 RESULTS AND DISCUSSION

The welding experiments employed some simple parameters, including a constant plunge rate of 50 mm/min and a plunge depth of 2.4 mm. The Si_3N_4 tool had a shoulder diameter of 10 mm and a pin length of 2 mm. Lap shear fracture loads and vertical welding loads are shown as a function of tool rpm in Table 1.

Table 1: Results from welding experiments, as a function of tool speed (RPM). An average of three specimens were taken in each case.

Tool RPM	Lap Shear Fracture Load (kN)	Vertical Welding Load (kN)
4000	7.2	4.7
5000	6.9	5.8
6000	7.8	3.9

The finite element model was used to simulate the three conditions from Table 1. The model employed 12,543 linear triangle elements for the sheets and 4,695 linear triangles for the tool. The two sheets were modeled as one body, for simplicity, but the joint interface was tracked with numerical sensors, in order to predict its movement during welding. The number of elements in the sheet mesh varied somewhat during the course of the simulation, because the sheet was automatically remeshed when element distortion reached a prescribed level. The backing plate was assumed to be rigid and at a constant temperature of 25°C, since the mass of the backing plate was relatively large compared to the mass of the sheet, and because the welding cycle only lasted for 2.3 seconds. The heat transfer coefficient between the lower sheet and the backing plate and between the tool and the tool holder was 20,000 W/m^2-°C, the friction coefficient was 0.1, and the plunge rate was a constant 50 mm/min. Temperature profiles for 4000, 5000, and 6000 rpm are shown in Figure 1 at the end of the welding process, where a section of the right half of the model is shown.

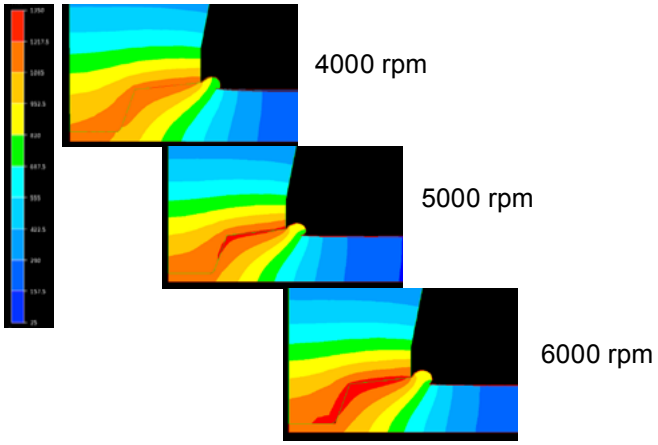

Figure 1: Temperature profiles at the end of welding, for 4000, 5000, and 6000 rpm tool speeds. The temperature scale goes from 25°C (dark blue) to 1350°C (red).

Thermocouple measurements for each experiment provided temperatures under the center of the pin, between the sheet and backing plate, for comparison with simulated temperatures. The comparison is shown in Table 2.

Table 2: Comparison of simulated and measured welding temperatures.

Tool RPM	Temp. under pin – simulation (°C)	Temp. under pin – measurement (°C)
4000	1109	1261
5000	1129	1403
6000	1155	1359

Measured temperatures were 150-274°C higher than the simulated temperatures, which may be caused by the imposed boundary condition at the backing plate. Further work on boundary conditions is needed in order to improve the prediction, although the discrepancy could also be caused by measurement error. In terms of material flow, the interface between the two sheets was tracking by numerical sensors, whose positions were updated after each increment of calculation. The simulated virtual interface, and comparison with experiment, is shown in Figure 2.

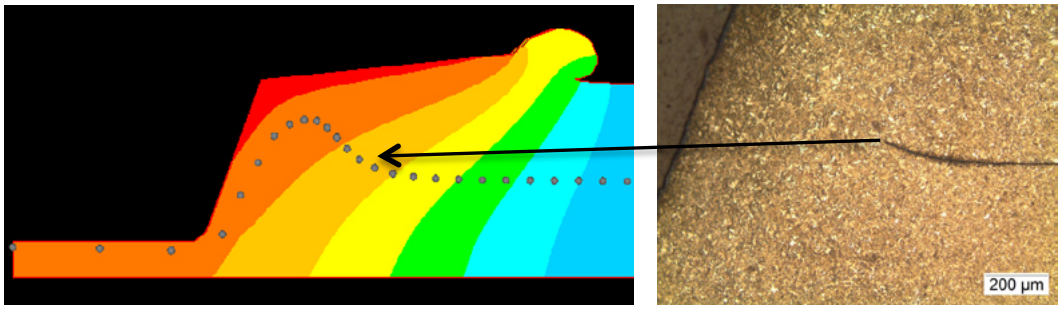

Figure 2: Simulated interface (left) and experimental interface (right) for tool speed of 5000 rpm. The predicted interface shows a rise in a similar location to the experiment. In the experiment, the interface vanishes where bonding has occurred.

In addition to predicting movement of the interface, the simulations were used to estimate where hardening of the weld occurred. For DP 980 steel, the austenite transformation temperature is about 900°C. The simulation predicted the areas in the weld where this threshold temperature was exceeded, and then a microhardness map was done on a weld cross section to show where the weld was harder than the base material (essentially indicating where portions of the weld transformed to austenite before cooling). The model prediction is compared to a microhardness map in Figure 3.

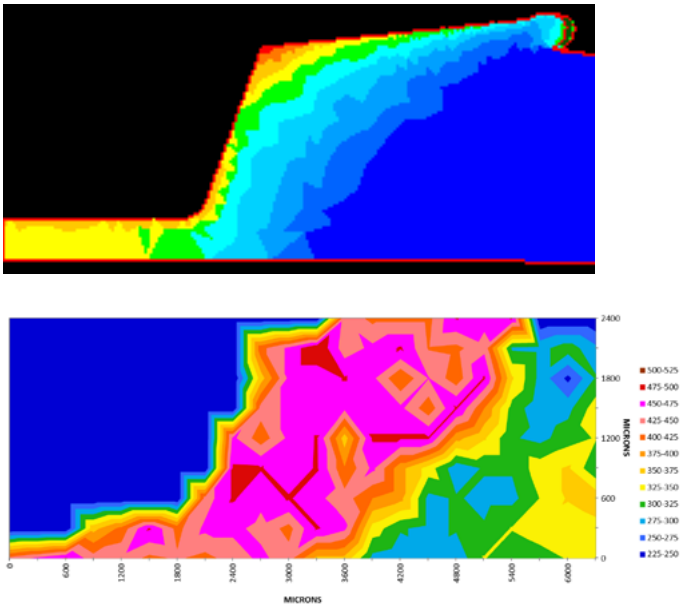

Figure 3: Prediction of areas of the weld which exceeded 900°C during welding (top). The dark blue areas did not exceed 900°C, while all other shaded areas did for various lengths of time. The microhardness map of a weld cross section (below) shows reasonable agreement with simulation, where the pink and red areas of the weld are harder than the base material (shown in yellow), indicating areas which would have transformed to austenite before cooling. The lighter blue and green areas in the microhardness map indicate material that underwent softening during the welding process.

There is a reasonable agreement between the areas of the microhardness map that indicate a transformation to austenite, and the areas of the weld predicted by simulation to exceed the austenite transition temperature.

5 CONCLUSIONS

A two dimensional, axisymmetric finite element model of friction stir spot welding was developed. The temperatures in the weld zone predicted by the model were less than those measured in an experiment. This discrepancy was likely caused by the boundary conditions imposed by the backing plate, although the temperature measurements could also be in error, as they are very difficult to make in such severe conditions. The final position of the interface between the sheets was predicted reasonably well, and this information will be related to joint performance in the future. Finally, the model predicted the hard zone in the weld qualitatively, by mapping the temperatures in the weld that exceeded the austenite transition temperature. Further refinement of the model will target predictions of weld bond area based on temperatures, pressures, and welding time.

6 ACKNOWLEDGMENT

This work was supported by National Science Foundation grant CMMI-1131203 and by funding from Department of Energy PNNL subcontract 116126.

7 REFERENCES

1. Bhadeshia, H.K.D.H. and T. DebRoy, *Critical assessment: friction stir welding of steels.* Science and Technology of Welding and Joining, 2009. **14**(3): p. 193-196.
2. Miles, M.P., et al., *Comparison of formability of friction stir welded and laser welded dual phase 590 steel sheets.* Science and Technology of Welding and Joining, 2006. **11**(4): p. 384-388.
3. Miles, M.P., et al., *Effect of friction stir welding conditions on properties and microstructures of high strength automotive steel.* Science and Technology of Welding and Joining, 2009. **14**(3): p. 228-232.
4. Chung, Y.D., et al., *Friction stir welding of high carbon steel with excellent toughness and ductility.* Scripta Materialia, 2010. **63**(2): p. 223-226.
5. Chung, Y.D., et al., *Friction stir welding of hypereutectoid steel (SK5) below eutectoid temperature.* Science and Technology of Welding and Joining, 2009. **14**(3): p. 233-238.
6. Reynolds, A.P., et al., *Friction stir welding of DH36 steel.* Science and Technology of Welding and Joining, 2003. **8**(6): p. 455-460.
7. Santella, M., et al., *Friction stir spot welding of DP780 carbon steel.* Science and Technology of Welding and Joining, 2010. **15**(4): p. 271-278.
8. Hovanski, Y., M.L. Santella, and G.J. Grant, *Friction stir spot welding of hot-stamped boron steel.* Scripta Materialia, 2007. **57**(9): p. 873-876.
9. Hovanski, Y., M.L. Santella, and G.J. Grant. *Friction Stir Spot Welding of Advanced High Strength Steels*. in *2009 International Autobody Congress*. 2009. Troy, MI.
10. Ohashi, R., et al., *Friction Spot Joining of High Strength Steel Sheets for Automotives.* Welding in the World, 2009. **53**(5-6): p. 23-27.
11. Ohashi, R., et al., *Microstructural Characterization of High-Strength Steel Lap Joint Produced by Friction Spot Joining.* Metallurgical and Materials Transactions a-Physical Metallurgy and Materials Science, 2009. **40A**(9): p. 2033-2035.
12. Sato, Y.S., et al., *Characteristics of microstructure in ultrahigh carbon steel produced during friction stir welding.* Isij International, 2008. **48**(1): p. 71-76.
13. Sato, Y.S., et al., *Microstructural evolution of ultrahigh carbon steel during friction stir welding.* Scripta Materialia, 2007. **57**(6): p. 557-560.
14. Sato, Y.S., et al., *Evaluation of microstructure and properties in friction stir welded superaustenitic stainless steel.* Science and Technology of Welding and Joining, 2009. **14**(3): p. 202-209.
15. Mandal, S., J. Rice, and A.A. Elmustafa, *Experimental and numerical investigation of the plunge stage in friction stir welding.* Journal of Materials Processing Technology, 2008. **203**(1-3): p. 411-419.
16. Awang, M. and V.H. Mucino, *Energy Generation during Friction Stir Spot Welding (FSSW) of Al 6061-T6 Plates.* Materials and Manufacturing Processes, 2010. **25**(1-3): p. 167-174.
17. Transvalor, S.A., *Forge 2009*, 2009.
18. Miles, M., et al. *Steady-State Simulation of Material Flow and Temperature in Friction Stir Welding of Aluminum Alloy 6061*. in *Materials Science & Technology 2008 - Joining of Advances and Specialty Metals*. 2008. Pittsburgh, PA.